

# **Enhancing the success rates by performing pooling decisions adjacent to the output layer**

**Yuval Meir<sup>1</sup>, Yarden Tzach<sup>1</sup>, Ronit D. Gross<sup>1</sup>, Ofek Tevet<sup>1</sup>, Roni Vardi<sup>2</sup> and Ido Kanter<sup>1,2,\*</sup>**

<sup>1</sup>Department of Physics, Bar-Ilan University, Ramat-Gan, 52900, Israel.

<sup>2</sup>Gonda Interdisciplinary Brain Research Center, Bar-Ilan University, Ramat-Gan, 52900, Israel.

\*Corresponding author email: ido.kanter@biu.ac.il

**Learning classification tasks of  $(2^n \times 2^n)$  inputs typically consist of  $\leq n$   $(2 \times 2)$  max-pooling (MP) operators along the entire feedforward deep architecture. Here we show, using the CIFAR-10 database, that pooling decisions adjacent to the last convolutional layer significantly enhance accuracy success rates (SRs). In particular, average SRs of the advanced-VGG with  $m$  layers (A-VGG $m$ ) architectures are 0.936, 0.940, 0.954, 0.955, and 0.955 for  $m=6, 8, 14, 13$ , and 16, respectively. The results indicate A-VGG8's SR is superior to VGG16's, and that the SRs of A-VGG13 and A-VGG16 are equal, and comparable to that of Wide-ResNet16. In addition, replacing the three fully connected (FC) layers with one FC layer, A-VGG6 and A-VGG14, or with several linear activation FC layers, yielded similar SRs. These significantly enhanced SRs stem from training the most influential input-output routes, in comparison to the inferior routes selected following multiple MP decisions along the deep architecture. In addition, SRs are sensitive to the order of the non-commutative MP and average pooling operators adjacent to the output layer, varying the number and location of training routes. The results call for the reexamination of previously proposed deep architectures and their SRs by utilizing the proposed pooling strategy adjacent to the output layer.**

## Introduction:

Classification tasks are typically solved using deep feedforward architectures<sup>1-6</sup>. These architectures are based on consecutive convolutional layers (CLs) and terminate with a few fully connected (FC) layers, in which the output layer size is equal to the number of input object labels. The first CL functions as a filter revealing a local feature in the input, whereas consecutive CLs are expected to expose complex, large-scale features that finally characterize a class of inputs<sup>1,7-9</sup>.

The deep learning strategy is efficient only if each CL consists of many parallel filters, the layer's depth, which differ by their initial convolutional weights. The depth typically increases along the deep architecture, resulting in enhanced accuracy success rates (SRs). In addition, given a deep architecture and the ratios between the depths of consecutive CLs, SRs increase as a function of the first CL depth<sup>10</sup>.

The deep learning strategy resulted in several practical difficulties, including the following. First, although the depth increases along the deep architecture, the input size of the layers remains fixed. The second difficulty is that the last CL output size, depth  $\times$  layer input size, becomes very large, serving as the first FC layer input, which consists of a large number of tunable parameters. These computational complexities overload even powerful GPUs, limited by the accelerated utilization of a large number of filters and sizes of the FC layers. One way to circumvent these difficulties is to embed pooling layers along the CLs<sup>1</sup>. Each pooling reduces the output dimension of a CL by combining a cluster of outputs, e.g.,  $2 \times 2$ , at one, and  $n$  such operations along the deep architecture reduce the CL dimension by a factor  $4^n$ . The most popular pooling operators are max-pooling (MP)<sup>11</sup>, which implements the maximal value of each cluster, and average pooling (AP)<sup>12,13</sup>, which implements the average value of each cluster; however, more types of pooling operators exist<sup>11,14-16</sup>.

The core question in this work is whether SRs can be enhanced depending on the location of the pooling operators along the CLs of a given deep architecture. For instance, VGG16 consists of 13 CLs, three FC layers, and five  $(2 \times 2)$  MP

operators located along the CLs<sup>2</sup> (Fig. 1A). The results indicate that SRs can be significantly increased by a smaller number of pooling operators adjacent to the last CL with optionally larger pooling sizes, for example, the advanced VGG16 (Fig. 1B). The optimized SRs of these types of advanced VGG architectures with  $m$  layers (A-VGG $m$ ) are first presented for selected  $m$  values ( $6 \leq m \leq 16$ ). Next, the underlying mechanism of the enhanced A-VGG $m$  SRs is discussed.

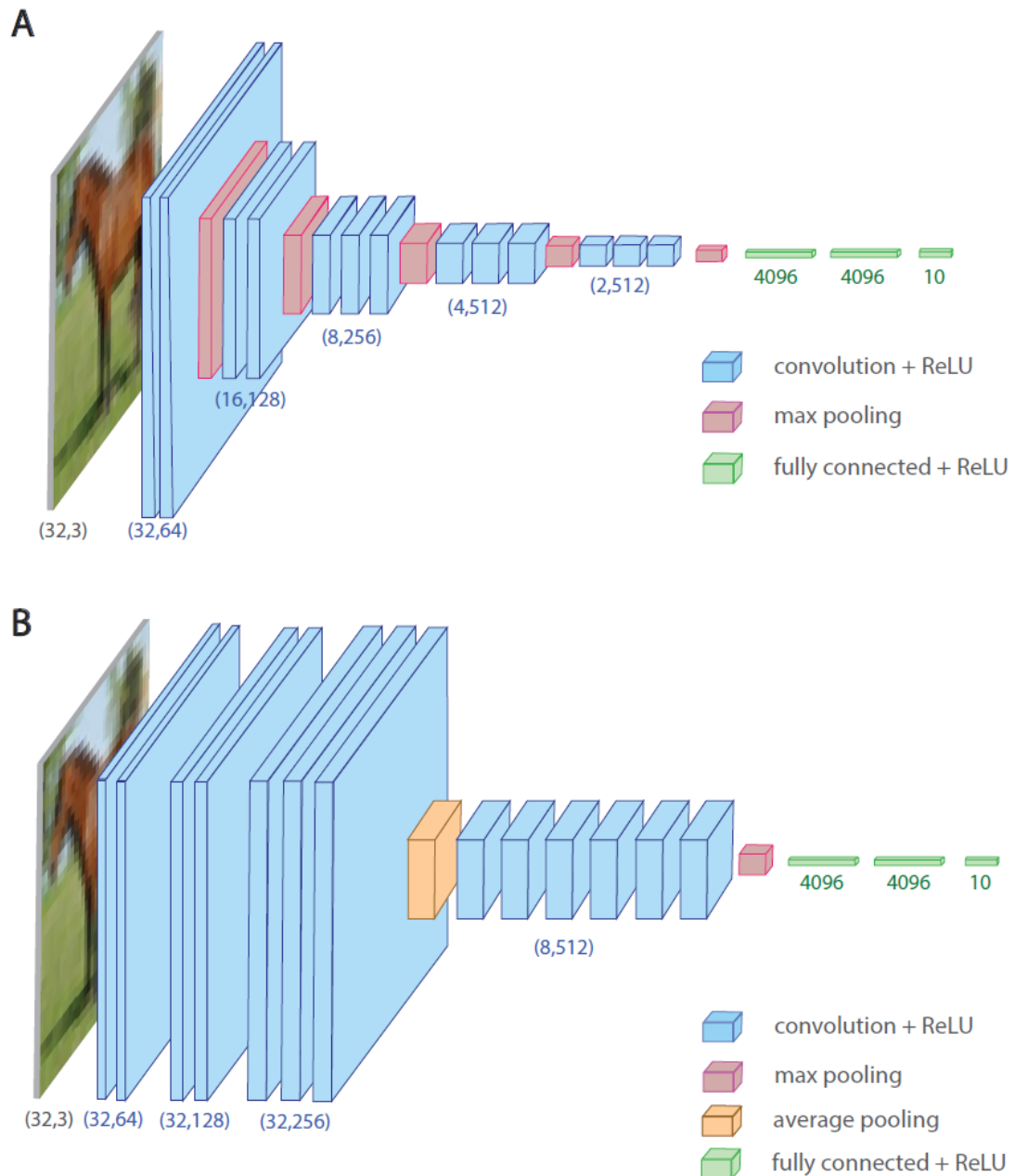


**Figure 1: VGG16 and A-VGG16 architectures. (A)** VGG16 architecture (13  $(3 \times 3)$  CLs and in between 5  $(2 \times 2)$  MP operators, followed by 3 FC layers) for the CIFAR10 database consisting of  $32 \times 32$  RGB inputs. A CL is defined by its square filters with dimension  $K$  and depth  $D$ ,  $(K, D)$ . **(B)** A-VGG16 architecture for CIFAR10 inputs consisting of 7  $(3 \times 3)$  CLs,  $(4 \times 4)$  average pooling (AP), 6  $(3 \times 3)$  CLs,  $(2 \times 2)$  MP and 3 FC layers.

### A-VGGm success rates:

A-VGG16 consists of  $(4 \times 4)$  average pooling (AP) and  $(2 \times 2)$  MP after the 7<sup>th</sup> and 13<sup>th</sup> CL, respectively (Fig. 1B and Table 1), with a maximal depth of 512 as in VGG16. The maximum average SR, 0.955, is superior to the optimized SR, 0.935, obtained for the standard VGG16<sup>10,17</sup> (Fig. 1A) and is comparable with the Wide-ResNet<sup>4,5</sup> median SR consisting of 16 layers with widening factor 10 (WRN16-10).

Note that the replacement of the pair of pooling operators,  $[AP(4 \times 4), MP(2 \times 2)]$  along A-VGG16 (Fig. 1B), by several other options, for example,  $[MP(2 \times 2), AP(4 \times 4)]$  and  $[AP(2 \times 2), MP(8 \times 8)]$ , also yielded an average SRs  $> 0.95$ , indicating the superior robustness of A-VGG16 SRs over VGG16. Removing the last three CLs (the fifth block of A-VGG16) resulting in A-VGG13, with an average SR of 0.955, identical to that of A-VGG16 up to the first three leading digits (Table 1). This suggests that SRs are only mildly affected by  $m > 16$ .

The A-VGG8 architecture that consists of only 8 layers, results in 0.940 averaged SR, exceeding the optimized VGG8 SR of 0.915, which consists of 5  $MP(2 \times 2)$  one after each CL<sup>2,18</sup>, and also exceeds the average SR of VGG16. Here again,  $AP(2 \times 2)$  and  $MP(4 \times 4)$  were placed after the 3<sup>rd</sup> and the 5<sup>th</sup> CLs, respectively (Table 1). This result indicates that a shallow architecture, with fewer pooling operators adjacent to the output, can imitate the SRs of a deeper architecture with double the number of layers.

Using only one FC layer reduces the number of layers by two, from A-VGG16 to A-VGG14, and from A-VGG8 to A-VGG6 (Table 1). The results indicate that

SRs are only mildly affected by such modifications, where A-VGG6 achieves an average SR of 0.936, which slightly exceeds that of VGG16 and A-VGG14 exceeds 0.954 (Table 1). We note that this type of architectures with only one FC layer consists of fewer parameters and can be mapped onto tree architectures, which will be discussed in another study<sup>19</sup>.

Similarly, the A-VGG13 and A-VGG16 architectures with linear activation functions for the FC layers achieved similar averaged SRs of 0.954 and 0.955, respectively, both with small standard deviations (Supplementary Information). The three linear FC layers can be folded into one in the test procedure<sup>20</sup>, minimizing its latency; however, training must be performed with three separated FC layers.

The gap between the average SRs of A-VGG8 and A-VGG6 ( $\sim 0.004$ ) was slightly greater than that between the enhanced SRs of A-VGG16 and A-VGG14 (Table 1), indicating that the gap decreases with  $m$ . Nevertheless, the comparable average SRs of A-VGG13 and A-VGG14 with A-VGG16 indicate that removing two out of three FC layers or removing three out of the thirteen CLs does not affect SRs. Hence, it is interesting to examine the average SRs of VGG11 where two FC layers as well as the last three CLs are removed.

A-VGG-6	A-VGG-8	A-VGG-13	A-VGG-14	A-VGG-16
Conv.1-64	Conv.1-64	Conv.2-64	Conv.2-64	Conv.2-64
Conv.1-128	Conv.1-128	Conv.2-128	Conv.2-128	Conv.2-128
Conv.1-256	Conv.1-256	Conv.3-256	Conv.3-256	Conv.3-256
AP 2x2	AP 2x2	AP 4x4	AP 4x4	AP 4x4
Conv.2-512	Conv.2-512	Conv.3-512	Conv.6-512	Conv.6-512
MP 8x8	MP 4x4	MP 4x4	MP 2x2	MP 2x2
FC x10	FC 8192	FC x2048	FC x10	FC x4096
	FC 8192	FC x2048		FC x4096
	FC x10	FC x10		FC x10
<b>Avg. Success Rate</b>				
0.936	0.940	0.955	0.954	0.955

**Table 1: Architectures and SRs of A-VGGm.** A-VGGm architectures,  $m=6, 8, 13, 14$ , and  $16$ , and their maximized average SRs obtained from 10 samples

(detailed parameters and SRs' standard deviations are presented in the Supplementary Information).

### **Optimized learning gain using pooling operators:**

The backpropagation learning step<sup>21</sup> updates the weights towards the correct output values for a given input. Typically, such a learning step can add noise and is destructive to a fraction of the training set<sup>22-25</sup>. However, the average SR increases with epochs and asymptotically saturates at a value that identifies the quality of the learning algorithm for a given architecture and database.

Another learning strategy is to update the weights belonging to the most influential routes on the output units only, that is, routes terminating with the maximal fields on the output units. Its underlying logic is to maximize the learning step gain for the current input while minimizing the added noise by zeroing other routes; *maximize learning with minimal side-effect damage*. The MP operator is an efficient way to implement this strategy. It selects the most influential weight from a small cluster on a node in the successive layer, for example, MP ( $2 \times 2$ ). Commonly, several MP operators are placed among the CLs, for example, five times in the case of VGG16 (Fig. 1A), and apparently solve simultaneously the following two difficulties. First, although the depth,  $D$ , increases along the CLs (Fig. 1A), the input size,  $K$ , of the layers shrinks accordingly such that the output sizes of the CLs,  $K \times D$ , do not grow linearly with depth. Second, successive MP operators appear to select the most influential routes on the first FC layer, which is adjacent to the output layer. However, these local decisions following consecutive MP operators do not necessarily result in the most influential routes in the first FC layer, as elaborated below using a toy model.

Assume a binary tree in which the randomly selected nodal values are low, medium, or high (Fig. 2A). The tree output is equal to the branch with the maximal field, which is calculated as the product of its three nodal values. The first strategy is based on local decisions, similar to MP operators. For each node the maximal ancestor, among the two, is selected (gray circles in Fig. 2A), and the selected route is the one composed of gray nodes only, where its value is

$M \cdot M \cdot M$  (the brown branch in Fig. 2A). However, a global decision among the eight branches results in a maximal field  $H \cdot H \cdot L$  (green branch in Fig. 2A). This toy model indicates that a global decision differs from local decisions; however, the probability of such an event is unclear.

A more realistic model, imitating deep architectures (Fig. 1), is Gaussian random  $(1024 \times 1024)$  inputs followed by ten  $(3 \times 3)$  CLs with unity depth (Fig. 2B). Two scenarios, local decisions and a global decision, are discussed. In the first,  $(2 \times 2)$  MP operators are placed after each of the first  $n$  CLs (Fig. 2B top, exemplified  $n = 4$ ), where in the second one a single  $(2^n \times 2^n)$  MP operator is placed after the ten CLs (Fig. 2B bottom, exemplified  $n = 4$ ). For both scenarios, there are  $(2^{10-n} \times 2^{10-n})$  non-negative (ReLU) outputs, denoted by  $O_{SP}$  (Sequence Pooling), representing local decisions and  $O_{TP}$  (Top Pooling), representing a global decision. For a given  $n$ , the  $2^{10-n} \times 2^{10-n}$  ratios,  $O_{SP}/O_{TP}$ , were calculated and averaged over many Gaussian random inputs and several sets of ten randomly selected convolutional filters, which were identical for both scenarios. The probability  $P(\frac{O_{SP}}{O_{TP}} > 1)$  indicates that local decisions,  $n$  consecutive MPs, result in a larger output than a global decision, a single  $(2^n \times 2^n)$  MP (Supplementary Information). This probability rapidly decreased with  $n$ , possibly exponentially (Fig. 2C), and even for  $n = 2$  it was below 0.1.

The increase in CLs depth beyond unity does not qualitatively affect the probability  $P(\frac{O_{SP}}{O_{TP}} > 1)$ , as indicated by simulations of VGG8 with five consecutive  $(2 \times 2)$  MP operators after each CL and a single  $(32 \times 32)$  MP after five CLs. The same five random  $(3 \times 3)$  convolutions were used for both architectures, and the 512 ratios,  $\frac{O_{SP}}{O_{TP}}$  for the single output of each filter, were calculated. Averaging over CIFAR10 training inputs and several selected sets of fixed random convolutions results in  $O(10^{-3})$  for probability  $P(\frac{O_{SP}}{O_{TP}} > 1)$ .

The results clearly indicate that a global selection of the most influential routes in the first FC layer, that is, pooling adjacent to the output layer, is almost always superior to the selection following consecutive local pooling decisions. This

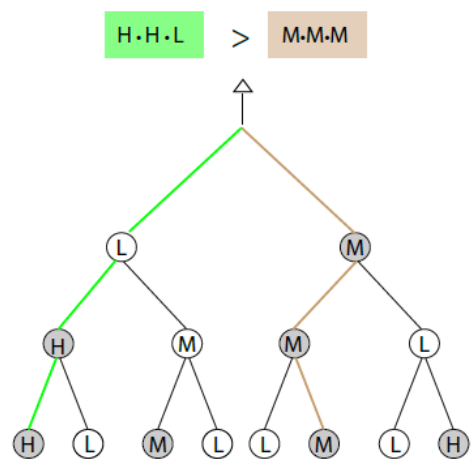
supports that using larger pooling operators adjacent to the output of the CLs enhances SRs (Table 1). It is expected that using pooling operators solely after the entire CLs will enhance SRs even further; however, its validation in simulations of A-VGGm architectures is difficult. The running time per epoch of such large  $K \times D$  deep architectures is several times longer, and the optimization of SRs is currently beyond our computational capabilities.

A simpler architecture is the LeNet5<sup>26,27</sup>, with much lower depth and total number of CLs, consisting of two CLs followed by  $(2 \times 2)$  MP each and three FC layers (Fig. 3A). The optimized average SR on the CIFAR10 database is 0.77.<sup>10</sup> Advanced LeNet5 (A-LeNet5) architectures consist of pooling operators only after the second CL (Fig. 3A). In particular, the two pooling options,  $(2 \times 2) AP \circ (2 \times 2) MP$  and  $(2 \times 2) MP \circ (2 \times 2) AP$  were examined (examples *a* and *b* in Fig. 3A), imitating the dimensions of the two  $(2 \times 2)$  MP of LeNet5. Indeed, these A-LeNet5 architectures enhance average SRs by up to  $\sim 0.02$ , in comparison to LeNet5 (Fig. 3B), as predicted by the abovementioned argument. Similarly, using either  $(4 \times 4) MP$  or  $(4 \times 4) AP$  after the second FC layer resulted in  $\sim 0.79$  maximized average SRs (not shown). The shift of the MP by only one CL, from the first to the second, improves the SRs, and an enhanced effect might be expected by skipping over more CLs in deeper architectures (Fig. 2C).

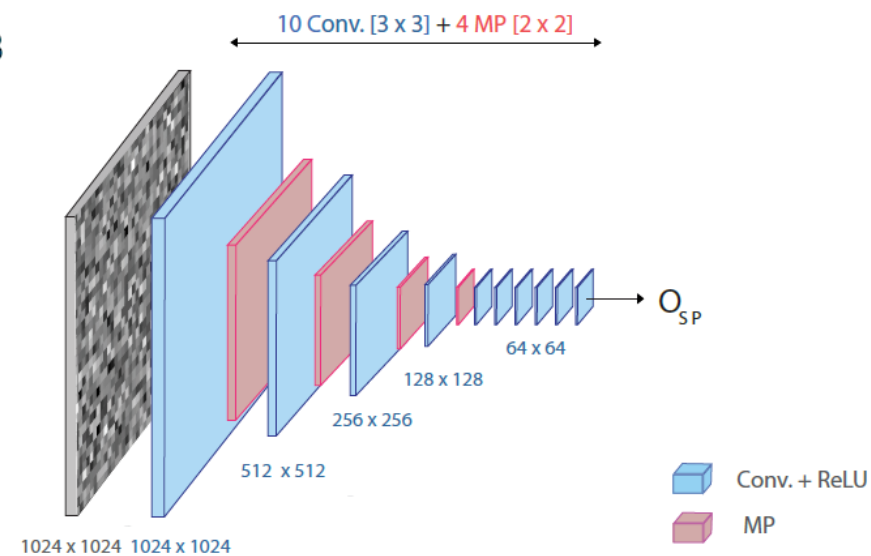
Another type of A-LeNet5 is a combination of a pair of  $(2 \times 2)$  and  $(3 \times 3)$  pooling operators after the two CLs (*c*, *d* and *e* in Fig. 3A). Although the input size of the first FC layer decreased from 400 in LeNet5 to 256, the average SRs was enhanced by  $\sim 0.011$  (*d* in Fig. 3B). This result exemplifies the improved A-LeNet5 SRs even when the input size of the first FC layer decreases. Examples *d* and *e* (Fig. 3A) consist of the same pooling operators,  $(2 \times 2) AP$  and  $(3 \times 3) MP$ , but with the exchanged order of the operators. Their average SRs differ by  $\sim 0.016$  (Fig. 3B), indicating that these pooling operators do not commute with the exchanged order. Another possible class of commutation is the exchanged type of operation (color) while maintaining their size; exchanged *MP* and *AP* (*d* and *e* in Fig. 3A). Average SRs indicate that pooling operators do not necessarily commute with exchanged colors.

The two non-commutative classes, order and type of operations, stem from different numbers and locations of the backpropagation active routes in the lower layers (Fig. 3C). The number of locally active backpropagation routes in a  $(6 \times 6)$  window is 9 for  $(3 \times 3) AP \circ (2 \times 2) MP$ , whereas for  $(3 \times 3) MP \circ (2 \times 2) AP$  is 4. For the exchanged order of operators ( $d$  and  $e$  in Fig. 3A), the number of backpropagation active routes is the same, 4, in both cases. However, these 4 routes were localized in  $(2 \times 2)$  ( $e$  in Fig. 3B and Fig. 3C), but delocalized over  $(6 \times 6)$  ( $d$  in Fig. 3B and Fig. 3C). Hence, the non-commutation of pooling operators can stem either from the different numbers of active backpropagation routes or from their different locations.

**A**



**B**



**C**

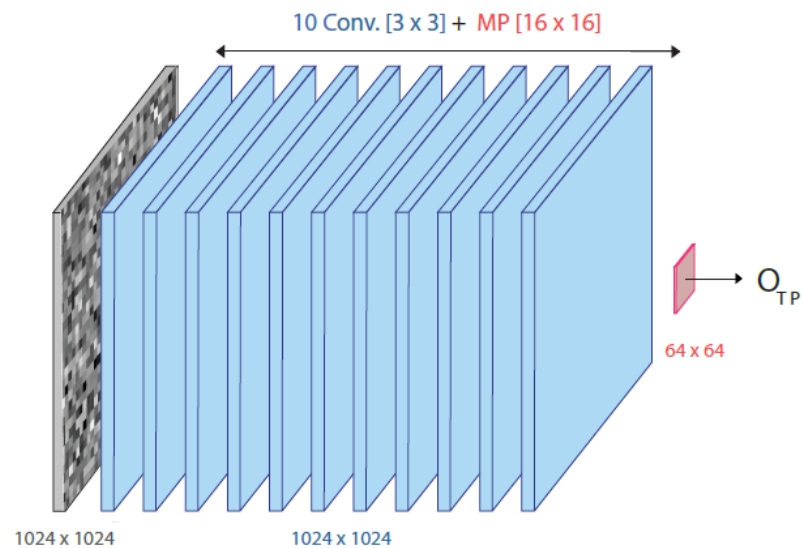
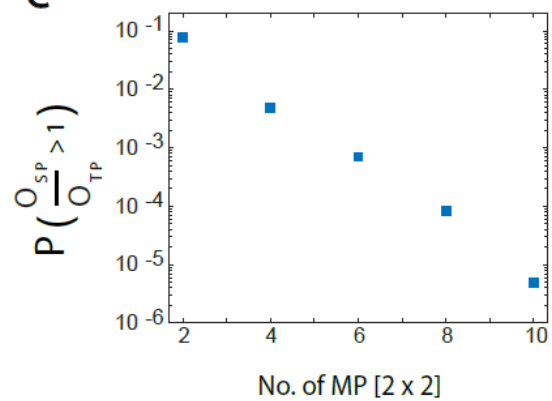


**Figure 2: Comparison between several small MP operators along CLs and a large one at their end. (A)** A binary tree where the randomly selected nodal values are low (L), medium (M), or high (H), e.g., 1, 10, and 1000. A local decision selects the maximal nodal ancestor (gray), and the brown route connects three gray nodes. A global decision selects the green route, maximizing the product of its nodal values. **(B)** Gaussian random ( $1024 \times 1024$ ) input followed by ten ( $3 \times 3$ ) CLs, where ( $2 \times 2$ ) MP is placed after the first four CLs (Top), and similar architecture where a single ( $16 \times 16$ ) MP is placed after the 10 CLs. The ( $64 \times 64$ ) output values are denoted by  $O_{SP}$  (Top) and  $O_{TP}$  (bottom) (Supplementary Information). **(C)** The probability  $P(\frac{O_{SP}}{O_{TP}} > 1)$  as a function of the number,  $n$ , of ( $2 \times 2$ ) MP ( $n = 4$  is demonstrated in **B**).

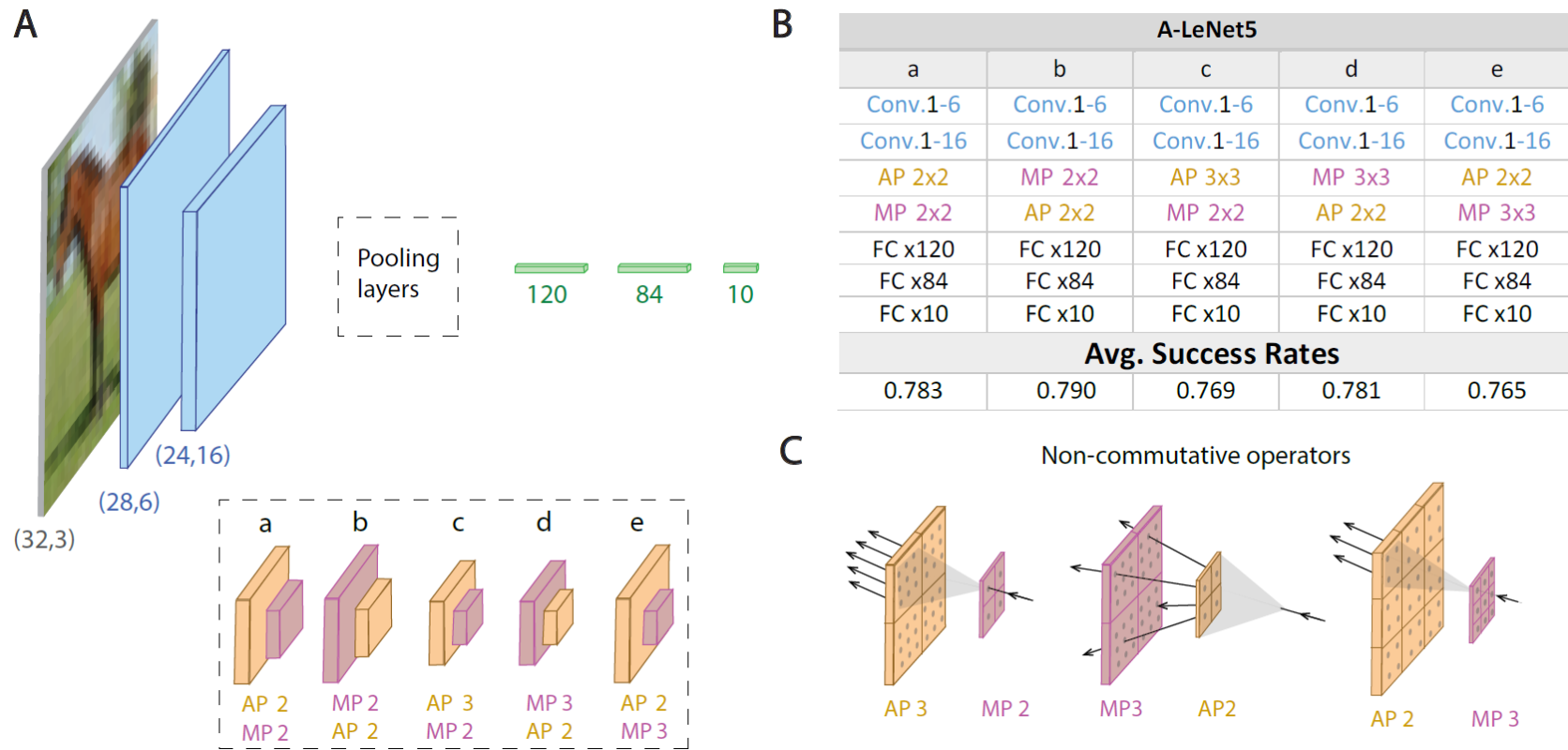


**Figure 3: A-LeNet5 SRs' architectures and the role of non-commutative pooling operators. (A)** A-LeNet5 architectures, where the pooling layers (exemplified in the dashed rectangle) are placed after the second CL. **(B)** Detailed architectures and average SRs for the five schemes of A-LeNet5 in **A** (see Supplementary Information for detailed parameters and standard deviations). **(C)** Non-commutative pooling operators, where the number of active backpropagation routes is 9 for  $(3 \times 3) AP \circ (2 \times 2) MP$ , 4 delocalized routes for  $(3 \times 3) MP \circ (2 \times 2) AP$  and 4 localized routes for  $(2 \times 2) AP \circ (3 \times 3) MP$ .

## Discussion:

The proposed enhanced learning strategy is based on updating the most influential routes, that is, the maximal fields, on the output units. This is supported by the A-VGGm and A-LeNet5 simulations, where the average SRs are enhanced using pooling operators placed closer to the output layer (Fig. 1, Table 1, and Fig. 3). Its underlying mechanism is aimed at maximizing the learning gain for the current input, while simultaneously minimizing the average damage on the current learning of the entire training set. Each learning step for a given input induces noise on the learning of other inputs. Hence, increasing the signal-to-noise ratio (SNR) of a learning step, average over the training set, requires updating the most influential routes of the current input; *maximize learning with minimal side-effect damage*.

The realization of the proposed advanced learning strategy entails a discussion of the following three theoretical and practical aspects. First, the selection of the most influential routes on the first FC layer is not necessarily equivalent to the selection of the most influential routes on the output units. However, a backpropagation step initiated at the most influential input weight on an output unit, updates all the CLs' routes since the spatial structure disappears within the one-dimensional FC layers. Hence, the proposed strategy approximates only the most influential routes on the outputs. The exceptional architectures were A-VGG6 and A-VGG14 (Table 1), consisting of one FC layer, demonstrating SRs that were only slightly below A-VGG8 and A-VGG16, respectively.

The second aspect concerns the computational complexity of the proposed advanced learning strategy. Selecting the most influential routes after all CLs with their fixed depth overloaded even advanced GPUs since the depth increases while the layer's dimension does not decrease. For instance, the running time per epoch of  $(32 \times 32)$  MP placed after all CLs of A-VGG16 was slowed down by a factor of  $\sim 10$ . To circumvent this difficulty, the advanced learning strategy was approximated by placing the first pooling operator before the CLs with maximal depth and the second operator after all CLs (Fig. 1 and Table 1). Nevertheless, it is interesting to examine, using advanced GPUs, whether placing pooling operators after all CLs further advances SRs.

The third aspect is the selection of the types, dimensions, and locations of pooling operators along the deep architecture to maximize SRs. For a given A-VGGm, several pooling arrangements result in similar SRs, and we report only the one that maximizes the average SRs under a given number of epochs. Nevertheless, the maximized average A-VGGm SRs hint at preferred combinations where the AP is placed before CLs with maximal depth and the MP operates after all CLs (Table 1 and Fig. 1), which might stem from the following insight. MP after all CLs carefully selects only one significant backpropagation route among a cluster of routes, whereas an AP close to the input layer spreads its incoming backpropagation signal to multiple routes. This arrangement was found to maximize SRs for several A-VGGm architectures (Table 1). However, A-LeNet indicated an opposite trend, where AP at the top of two adjacent pooling operators maximized SRs (Fig. 3). The role is not yet clear and may depend on the database and details of the training architecture.

The non-commutative pooling operator features exemplify the sensitivity of the maximal average SRs to their order and type, and significantly enrich the possible number of pooling operators with a given dimension. For  $(8 \times 8)$  pooling dimension, for instance, one can find 8 possible pooling operators;  $(2 \times 2)XP \circ (2 \times 2)YP \circ (2 \times 2)ZP$ , where  $X, Y$  and  $Z$  equal either to  $M$  (Max) or  $A$  (Average). Similarly, the number of pooling operators with dimension  $(2^n \times 2^n)$  is  $2^n$ , and exponentially increases when more than two types of  $(2 \times 2)$  pooling operators are allowed. The results for A-LeNet indicate that enhanced SRs can be achieved using combinations of consecutive pooling operators after the second CLs (Fig. 3). However, the identification of preferred combinations to maximize the SRs in general deep architectures deserves further research.

The non-commutative features of pooling operators also stem from their different number of backpropagation downstream updated routes (Fig. 3C). For instance, A-VGG16 with  $(32 \times 32)$  MP, before the first FC layer, consists of a single backpropagation downstream updated route per filter, whereas for  $(32 \times 32)$  AP there are 1024 routes. Nevertheless, the preferred pooling operators to maximize SRs need to be determined. The most influential route is favored to correct the output of the current input; however, it induces output

noise on other training inputs, resulting in a low SNR. Similarly, updating 1024 downstream routes using AP, including the weak ones, increases the correct output of the current input in comparison to MP; however, with enhanced side-effect, noise on other training inputs, resulting in a possibly low SNR. Hence, for a given architecture and dataset, the selection of pooling operators that maximize the averaged SNR per epoch is yet unclear.

The SRs of A-VGG6 and A-VGG14 with only one FC layer were only slightly below those of the three FC layers, A-VGG8 and A-VGG-16, respectively (Table 1). Architectures with only one FC layer are characterized by lower learning complexity and number of tunable parameters. In addition, these architectures can be mapped onto tree architectures<sup>28,29</sup>, generalizing recent LeNet mapping into tree architecture without affecting SRs but with lower computational learning complexity<sup>29</sup>. Tree mapping of architectures comprising more than two CLs, inspired by dendritic tree learning<sup>28-33</sup>, is beyond the scope of the presented work and will be discussed elsewhere<sup>19</sup>.

Finally, the reported average SRs for A-VGG16 and A-VGG13 approach Wide-ResNet16 (widening factor of 10) median SRs, consisting of an architecture with three main ingredients: skip connections, CLs with stride = 2 and  $(8 \times 8)$  AP after all CLs. This similarity hints that the ingredient dominating the enhanced SRs, among the three, is a pooling operation after all CLs.

**Data availability**

Source data were provided in this study. All data supporting the plots within this paper, along with other findings of this study, are available from the corresponding author upon reasonable request.

**Code availability**

The simulation code is provided in this study, parallel to its publication in GitHub.

**Acknowledgments**

I.K. acknowledges the partial financial support from the Israel Science Foundation (grant number 346/22).

**Author contributions**

Y.M., Y.T., R. D. G., and O.T. contributed equally to this study. R. V. discussed the results and commented on the manuscript. I.K. initiated and supervised all aspects of the study.

**Competing interests**

The authors declare no competing interests.

**Additional information**

Supplementary information. The online version contains supplementary material available at

- 1 LeCun, Y., Bengio, Y. & Hinton, G. Deep learning. *Nature* **521**, 436-444 (2015).
- 2 Simonyan, K. & Zisserman, A. Very deep convolutional networks for large-scale  
image recognition. *arXiv preprint arXiv:1409.1556* (2014).
- 3 Szegedy, C. et al. in *Proceedings of the IEEE conference on computer vision and  
pattern recognition*. 1-9.
- 4 Zagoruyko, S. & Komodakis, N. Wide residual networks. *arXiv preprint  
arXiv:1605.07146* (2016).
- 5 He, K., Zhang, X., Ren, S. & Sun, J. in *Proceedings of the IEEE conference on computer  
vision and pattern recognition*. 770-778.
- 6 Szegedy, C., Ioffe, S., Vanhoucke, V. & Alemi, A. in *Proceedings of the AAAI  
conference on artificial intelligence*.
- 7 Krizhevsky, A., Sutskever, I. & Hinton, G. E. Imagenet classification with deep  
convolutional neural networks. *Communications of the ACM* **60**, 84-90 (2017).
- 8 Hertel, L., Barth, E., Käster, T. & Martinetz, T. in *2015 International Joint Conference  
on Neural Networks (IJCNN)*. 1-4 (IEEE).
- 9 Wiatowski, T. & Bölcskei, H. A mathematical theory of deep convolutional neural  
networks for feature extraction. *Ieee T Inform Theory* **64**, 1845-1866 (2017).
- 10 Meir, Y. et al. Efficient shallow learning as an alternative to deep learning. *arXiv  
preprint arXiv:2211.11106* (2022).
- 11 Yu, D., Wang, H., Chen, P. & Wei, Z. in *Rough Sets and Knowledge Technology: 9th  
International Conference, RSKT 2014, Shanghai, China, October 24-26, 2014,  
Proceedings 9*. 364-375 (Springer).
- 12 LeCun, Y. et al. Handwritten digit recognition with a back-propagation network.  
*Advances in neural information processing systems* **2** (1989).
- 13 LeCun, Y., Bottou, L., Bengio, Y. & Haffner, P. Gradient-based learning applied to  
document recognition. *Proceedings of the IEEE* **86**, 2278-2324 (1998).
- 14 Hinton, G. E., Srivastava, N., Krizhevsky, A., Sutskever, I. & Salakhutdinov, R. R.  
Improving neural networks by preventing co-adaptation of feature detectors. *arXiv  
preprint arXiv:1207.0580* (2012).
- 15 Wan, L., Zeiler, M., Zhang, S., Le Cun, Y. & Fergus, R. in *International conference on  
machine learning*. 1058-1066 (PMLR).
- 16 Sermanet, P., Chintala, S. & LeCun, Y. in *Proceedings of the 21st international  
conference on pattern recognition (ICPR2012)*. 3288-3291 (IEEE).
- 17 Hasanpour, S. H., Rouhani, M., Fayyaz, M., Sabokrou, M. & Adeli, E. Towards  
principled design of deep convolutional networks: Introducing simpnet. *arXiv  
preprint arXiv:1802.06205* (2018).
- 18 Cai, Y. et al. Low bit-width convolutional neural network on RRAM. *IEEE Transactions  
on Computer-Aided Design of Integrated Circuits and Systems* **39**, 1414-1427 (2019).
- 19 al., Y. T. e. (unpublished).
- 20 Dror, A. B. et al. Layer Folding: Neural Network Depth Reduction using Activation  
Linearization. *arXiv preprint arXiv:2106.09309* (2021).
- 21 LeCun, Y. in *Computer Vision—ECCV 2012. Workshops and Demonstrations: Florence,  
Italy, October 7-13, 2012, Proceedings, Part I 12*. 496-505 (Springer).
- 22 Minsky, M. L. & Papert, S. A. (MIT press, 1988).
- 23 Gardner, E. The space of interactions in neural network models. *Journal of physics A:  
Mathematical and general* **21**, 257 (1988).
- 24 Kirkpatrick, J. et al. Overcoming catastrophic forgetting in neural networks.  
*Proceedings of the national academy of sciences* **114**, 3521-3526 (2017).
- 25 Kaushik, P., Gain, A., Kortylewski, A. & Yuille, A. Understanding catastrophic  
forgetting and remembering in continual learning with optimal relevance mapping.  
*arXiv preprint arXiv:2102.11343* (2021).

- 26     LeCun, Y. *et al.* Learning algorithms for classification: A comparison on handwritten digit recognition. *Neural networks: the statistical mechanics perspective* **261**, 2 (1995).
- 27     LeCun, Y. *et al.* Backpropagation applied to handwritten zip code recognition. *Neural Comput* **1**, 541-551 (1989).
- 28     Hodassman, S., Vardi, R., Tugendhaft, Y., Goldental, A. & Kanter, I. Efficient dendritic learning as an alternative to synaptic plasticity hypothesis. *Scientific Reports* **12**, 6571 (2022).
- 29     Meir, Y., Ben-Noam, I., Tzach, Y., Hodassman, S. & Kanter, I. Learning on tree architectures outperforms a convolutional feedforward network. *Sci Rep-Uk* **13**, 962 (2023).
- 30     Sardi, S. *et al.* Adaptive nodes enrich nonlinear cooperative learning beyond traditional adaptation by links. *Scientific reports* **8**, 5100 (2018).
- 31     Sardi, S. *et al.* Brain experiments imply adaptation mechanisms which outperform common AI learning algorithms. *Scientific reports* **10**, 6923 (2020).
- 32     Sardi, S. *et al.* Long anisotropic absolute refractory periods with rapid rise times to reliable responsiveness. *Physical Review E* **105**, 014401 (2022).
- 33     Uzan, H., Sardi, S., Goldental, A., Vardi, R. & Kanter, I. Biological learning curves outperform existing ones in artificial intelligence algorithms. *Sci Rep-Uk* **9**, 1-11 (2019).

## **Supplementary Information**

**Enhancing the success rates by performing pooling decisions adjacent to the output layer**

**Yuval Meir<sup>1</sup>, Yarden Tzach<sup>1</sup>, Ronit D. Gross<sup>1</sup>, Ofek Tevet<sup>1</sup>, Roni Vardi<sup>2</sup> and Ido Kanter<sup>1,2,\*</sup>**

<sup>1</sup>Department of Physics, Bar-Ilan University, Ramat-Gan, 52900, Israel.

<sup>2</sup>Gonda Interdisciplinary Brain Research Center, Bar-Ilan University, Ramat-Gan, 52900, Israel.

\*Corresponding author email: [ido.kanter@biu.ac.il](mailto:ido.kanter@biu.ac.il)

**Advanced VGGm architectures.** The examined advanced VGGm (A-VGGm) architectures consist of  $m$  layers,  $6 \leq m \leq 16$  (Fig. 1A-B, exemplifies  $m = 16$  for VGG16<sup>1</sup> and A-VGG16).

For  $m = 6$  and 8, the architecture is similar to the VGG8<sup>1</sup>, with initial depth of 64 for the first CL and doubling depth for the next three CLs, and with a single zero-padding around the input of each CL. For  $m = 6$ , a  $(2 \times 2)$  average pooling (AP) is applied after the third CL and an  $(8 \times 8)$  max-pooling (MP) after the fifth CL. For  $m = 8$ , a  $(2 \times 2)$  AP is applied after the third CL and a  $(4 \times 4)$  MP after the fifth CL.  $m = 6$  terminates with one FC layer consisting of 2048 hidden units and  $m = 8$  with three FC layers with 8192 hidden units each.

For  $m = 14$  and 16, there are 13 CLs with doubling depth (except for the last 3 CLs) and with a single zero-padding around the input of each CL, followed by one FC layer with 8192 hidden units for  $m = 14$  and three FC layers with 4096 hidden units for  $m = 16$ . For both  $m = 14$  and 16, a  $(4 \times 4)$  AP is applied after the 7<sup>th</sup> CL and a  $(2 \times 2)$  MP is applied after the 13<sup>th</sup> CL.

For  $m = 13$  the last three CLs are withdrawn, resulting in ten CLs, where a  $(4 \times 4)$  AP is also applied after the 7<sup>th</sup> CL and a  $(4 \times 4)$  MP is applied after the 10<sup>th</sup> CL terminating with three FC layers consisting of 2048 hidden units each.

After each CL, a batch normalization layer was applied. The softmax function was applied to the ten outputs. The ReLU activation function was assigned to each hidden unit (not including the ten output units and pooling operators), and all weights were initialized using a uniform distribution with a zero mean and unity standard deviation (Std) according to the He normal initialization<sup>3</sup>.

For A-VGG13 and A-VGG16 with linear activation functions for the FC layer the architectures remain the same.

**Advanced LeNet5 architectures.** The advanced LeNet5 (A-LeNet5) architectures consist of two consecutive CLs of size  $(5 \times 5)$  with depths  $d_1 = 6$  and  $d_2 = 16$  and three FC layers (Fig. 3A). These architectures are similar to the LeNet5<sup>2</sup>, however, the pooling operators are applied only after the second CL (Fig. 3A). The ReLU activation function was assigned to each hidden unit where the softmax function was applied to the ten output units. All weights were

initialized using a uniform distribution with a zero mean and unity Std according to the He normal initialization<sup>3</sup>.

**Data preprocessing.** Each input pixel of an image ( $32 \times 32$ ) from the CIFAR-10 database was divided by the maximal pixel value, 255, multiplied by 2, and subtracted by 1, such that its range was  $[-1, 1]$ . In all simulations, data augmentation was used, derived from the original images, by random horizontally flipping and translating up to four pixels in each direction.

**Optimization.** The cross-entropy cost function was selected for the classification task and was minimized using the stochastic gradient descent algorithm<sup>4,5</sup>. The maximal accuracy was determined by searching through the hyper-parameters (see below). Cross-validation was confirmed using several validation databases, each consisting of 10,000 random examples from the training set, as in the test set. The averaged results were in the same Std as the reported average success rates. The Nesterov momentum<sup>3</sup> and L2 regularization method<sup>4</sup> were applied.

**Hyper-parameters.** The hyper-parameters  $\eta$  (learning rate),  $\mu$  (momentum constant<sup>3</sup>), and  $\alpha$  (regularization L2<sup>4</sup>) were optimized for offline learning, using a mini-batch size of 100 inputs. The learning rate decay schedule<sup>5,6</sup> was also optimized such that it was multiplied by the decay factor,  $q$ , every  $\Delta t$  epochs, and is denoted below as  $(q, \Delta t)$ .

**Out of phase scheduling.** For A-VGG16 and A-VGG8 the decay schedules<sup>5,6</sup> of the FC layers and the CLs learning rates had a phase of 10 epochs in between. The decay scheduling for the FC layers starts at epoch = 10, while for the CLs at epoch = 20. Specifically, decay learning rate of the FC layers occurs at epochs =  $[10, 30, 50 \dots]$ , while for the CLs at epochs =  $[20, 40, 60 \dots]$ .

**Fig 1. A-VGGm Hyper-parameters**

A-VGG16				
Layer	$\eta$	$\mu$	$\alpha$	epochs
CLs	0.00721	0.98	1.15e-3	280
FC layers	0.0045	0.982	1.35e-3	280

The decay schedule for the learning rate is defined as follows:

For CLs:

$$(q, \Delta t) = \begin{cases} (0.65, 20) & \text{epoch} \leq 140 \\ (0.55, 20) & \text{epoch} > 140 \end{cases}$$

For FC layers, with 10 epochs out of phase:

$$(q, \Delta t) = \begin{cases} (0.65, 20) & \text{epoch} < 150 \\ (0.5, 20) & \text{epoch} \geq 150 \end{cases}$$

The SRs' Std is 0.0015.

<b>A-VGG14</b>				
Layers	$\eta$	$\mu$	$\alpha$	epochs
CLs	0.0078	0.985	1.15e-3	200
FC layers	6.05e-4	0.98	1.15e-3	200

The decay schedule for the learning rate is defined as follows:

For CLs:

$$(q, \Delta t) = (0.65, 20)$$

For FC layers:

$$(q, \Delta t) = \begin{cases} (0.55, 10) & \text{epoch} < 120 \\ (0.5, 10) & \text{epoch} \geq 120 \end{cases}$$

The SRs' Std is 0.00092.

<b>A-VGG13</b>				
Layers	$\eta$	$\mu$	$\alpha$	epochs
CLs	0.0078	0.98	1.15e-3	200
FC layers	0.00297	0.985	1.15e-3	200

The decay schedule for the learning rate is defined as follows:

For CLs:

$$(q, \Delta t) = (0.65, 20)$$

For FC layers:

$$(q, \Delta t) = \begin{cases} (0.55, 20) & \text{epoch} < 120 \\ (0.5, 20) & \text{epoch} \geq 120 \end{cases}$$

The SRs' Std is 0.0012.

<b>A-VGG8</b>				
Layers	$\eta$	$\mu$	$\alpha$	epochs
CLs	0.0145	0.97	1e-3	200
FC layers	0.002	0.975	1.2e-3	200

The decay schedule for the learning rate is defined as follows:

For CLs:

$$(q, \Delta t) = \begin{cases} (0.66, 20) & \text{epoch} \leq 140 \\ (0.55, 20) & \text{epoch} > 140 \end{cases}$$

For FC layers with 10 epochs out of phase:

$$(q, \Delta t) = \begin{cases} (0.66, 20) & \text{epoch} < 150 \\ (0.5, 20) & \text{epoch} \geq 150 \end{cases}$$

The SRs' Std is 0.0009.

<b>A-VGG6</b>				
Layers	$\eta$	$\mu$	$\alpha$	epochs
CLs	9.75e-3	0.972	1.1e-3	200
FC layers	1.95e-3	0.98	1.1e-3	200

The decay schedule for the learning rate is defined as follows:

For CLs:

$$(q, \Delta t) = \begin{cases} (0.65, 20) & \text{epoch} < 120 \\ (0.55, 20) & \text{epoch} \geq 120 \end{cases}$$

For FC layers:

$$(q, \Delta t) = \begin{cases} (0.65, 20) & \text{epoch} < 120 \\ (0.5, 20) & \text{epoch} \geq 120 \end{cases}$$

The SRs' Std is 0.00224.

**A-VGG13 and A-VGG16 with linear activation functions for the FC layers.**

<b>A-VGG16 with linear activation</b>				
Layer	$\eta$	$\mu$	$\alpha$	epochs
CLs	0.0078	0.98	1.15e-3	200
FC layers	0.00297	0.985	1.15e-3	200

The decay schedule for the learning rate is defined as follows:

For CLs:

$$(q, \Delta t) = (0.65, 20)$$

For FC layers:

$$(q, \Delta t) = \begin{cases} (0.55, 20) & \text{epoch} < 120 \\ (0.5, 20) & \text{epoch} \geq 120 \end{cases}$$

The SRs' Std is 0.0014.

<b>A-VGG13 with linear activation</b>				
Layer	$\eta$	$\mu$	$\alpha$	epochs
CLs	0.0078	0.98	1.15e-3	200
FC layers	0.00297	0.985	1.15e-3	200

The decay schedule for the learning rate is defined as follows:

For CLs:

$$(q, \Delta t) = (0.65, 20)$$

For FC layers:

$$(q, \Delta t) = \begin{cases} (0.55, 20) & \text{epoch} < 120 \\ (0.5, 20) & \text{epoch} \geq 120 \end{cases}$$

The SRs' Std is 0.001.

**Fig. 2.** In Fig. 2, two architectures were compared, each consists of ten CLs with unity depth and the same ten  $(3 \times 3)$  filters. Random inputs of size  $(1024 \times 1024)$  with values taken from a Gaussian distribution with zero mean and unity Std were tested. The ReLU activation function was assigned to all the hidden and output units.

Two architectures were compared, sequence pooling (SP) and top pooling (TP). The SP architecture consists of  $(2 \times 2)$  MP after each one of the first  $n$  CLs, whereas for the TP architecture  $(2^n \times 2^n)$  MP is applied after the 10<sup>th</sup> CL (Fig. 2B top, exemplifies  $n = 4$ ). For a given  $n = [2, 4, 6, 8, 10]$ , the  $(2^{10-n} \times 2^{10-n})$  SP and TP output ratios,  $\frac{O_{SP}}{O_{TP}}$ , were calculated and the probability  $P\left(\frac{O_{SP}}{O_{TP}} > 1\right)$  was estimated using 20,000 - 100,000 different random inputs (depending on  $n$ ), and filters which were randomly initialized for the CLs on each sample.

The increase in CLs depth beyond unity does not qualitatively affect  $P\left(\frac{O_{SP}}{O_{TP}} > 1\right)$ , as indicated by simulations of VGG8 with five consecutive  $(2 \times 2)$  MP operators after each CL and a single  $(32 \times 32)$  MP after five CLs. The same five random  $(3 \times 3)$  convolutions were used for both architectures, and the 512 ratios,  $\frac{O_{SP}}{O_{TP}}$ , for the single output of each filter, were calculated. The probability  $P\left(\frac{O_{SP}}{O_{TP}} > 1\right)$  was calculated by averaging over randomly selected batches of CIFAR10 training inputs and several selected sets of fixed random convolutions.

**Fig 3. A-LeNet5 Hyper-parameters**

A-LeNet5 - a			
$\eta$	$\mu$	$\alpha$	epochs
0.032	0.92	5e-4	240

The decay schedule for the learning rate is defined as follows:

$$(q, \Delta t) = \begin{cases} (0.8, 10) & \text{epoch} < 120 \\ (0.7, 10) & \text{epoch} \geq 120 \end{cases}$$

The SRs' Std is 0.0028.

<b>A-LeNet5 - b</b>			
$\eta$	$\mu$	$\alpha$	epochs
0.03	0.93	4e-4	280

The decay schedule for the learning rate is defined as follows:

$$(q, \Delta t) = \begin{cases} (0.8, 10) & \text{epoch} < 120 \\ (0.7, 10) & \text{epoch} \geq 120 \end{cases}$$

The SRs' Std is 0.003.

<b>A-LeNet5 - c</b>			
$\eta$	$\mu$	$\alpha$	epochs
0.028	0.925	5e-4	280

The decay schedule for the learning rate is defined as follows:

$$(q, \Delta t) = \begin{cases} (0.8, 10) & \text{epoch} < 120 \\ (0.7, 10) & \text{epoch} \geq 120 \end{cases}$$

The SRs' Std is 0.0025.

<b>A-LeNet5 - d</b>			
$\eta$	$\mu$	$\alpha$	epochs
0.032	0.92	5e-4	240

The decay schedule for the learning rate is defined as follows:

$$(q, \Delta t) = \begin{cases} (0.8, 10) & \text{epoch} < 120 \\ (0.7, 10) & \text{epoch} \geq 120 \end{cases}$$

The SRs' Std is 0.0035.

A-LeNet5 - e			
$\eta$	$\mu$	$\alpha$	epochs
0.02	0.922	1.2e-3	240

The decay schedule for the learning rate is defined as follows:

$$(q, \Delta t) = \begin{cases} (0.8, 10) & \text{epoch} < 120 \\ (0.7, 10) & \text{epoch} \geq 120 \end{cases}$$

The SRs' Std is 0.0039.

**Statistics.** Statistics for each architecture were obtained using 10 samples.

**Hardware and software.** We used Google Colab Pro and its available GPUs. We used Pytorch for all the programming processes.

1. Simonyan, K. & Zisserman, A. Very Deep Convolutional Networks for Large-Scale Image Recognition. (2014).
2. LeCun, Y. *et al.* Backpropagation Applied to Handwritten Zip Code Recognition. *Neural Comput* **1**, 541–551 (1989).
3. Botev, A., Lever, G. & Barber, D. Nesterov's accelerated gradient and momentum as approximations to regularised update descent. in *2017 International Joint Conference on Neural Networks (IJCNN)* 1899–1903 (IEEE, 2017). doi:10.1109/IJCNN.2017.7966082.
4. Schmidhuber, J. Deep learning in neural networks: An overview. *Neural Networks* **61**, 85–117 (2015).
5. He, K., Zhang, X., Ren, S. & Sun, J. Deep Residual Learning for Image Recognition. (2015).
6. You, K., Long, M., Wang, J. & Jordan, M. I. How Does Learning Rate Decay Help Modern Neural Networks? (2019).